Atomic Layer Etching Using Thermal Reactions:
Atomic Layer Deposition in Reverse

Y. Lee[a], J.W. DuMont[a], and S.M. George[a,b]

[a] Department of Chemistry and Biochemistry, University of Colorado,
Boulder, Colorado, 80309, USA
[b] Department of Mechanical Engineering, University of Colorado,
Boulder, Colorado, 80309, USA

Atomic layer etching (ALE) can remove thin films with atomic layer control based on sequential, self-limiting surface reactions. ALE can be viewed as atomic layer deposition (ALD) in reverse. This paper reviews Al_2O_3 ALE using sequential, self-limiting thermal reactions. In the proposed mechanism for thermal Al_2O_3 ALE, fluorination reagents, such as HF, fluorinate the Al_2O_3 substrate to form an AlF_3 surface layer and volatile H_2O. A metal precursor, such as $Sn(acac)_2$, subsequently accepts fluorine from the AlF_3 surface layer and donates an acac ligand to the aluminum in the AlF_3 surface layer to form volatile $Al(acac)_3$ or $AlF(acac)_2$ reaction products. These fluorination and ligand-exchange reactions with HF and $Sn(acac)_2$ lead to temperature-dependent etching rates of Al_2O_3 from 0.14 Å/cycle at 150°C to 0.61 Å/cycle at 250°C. This reaction mechanism can be extended to a variety of other materials including metal nitrides, metal phosphides, metal arsenides and elemental metals.

Introduction

Atomic layer etching (ALE) is a thin film removal process based on sequential, self-limiting surface reactions [1-3]. ALE can be viewed as the reverse of atomic layer deposition (ALD) [3-5]. ALE is able to remove thin films with atomic layer control. ALD and ALE are able to provide the necessary tools for surface engineering at the atomic level [6, 7]. This atomic level control is required for the nanofabrication of nanoscale devices.

Previous ALE processes have used ion-enhanced or energetic neutral atom beam-enhanced surface reactions together with halogenation of the surface to etch the material. This ALE approach can produce anisotropic etching and has been used for the ALE of Si [8-11], Ge [12], compound semiconductors [13-16], metal oxides [17-21], and various carbon substrates [22-24]. In contrast to the large number of ALE processes performed using ion-enhanced or energetic neutral atom beams, there are very few ALE processes based on spontaneous thermal chemistry. These thermal ALE processes could be useful for the isotropic removal of thin films with atomic layer control [2].

The ALE of Al_2O_3 was recently reported using sequential, self-limiting thermal reactions with $Sn(acac)_2$ and HF as the reactants [25]. The linear removal of Al_2O_3 was observed at temperatures from 150-250°C without the use of ion or noble gas atom

bombardment. Al$_2$O$_3$ ALE etch rates varied with temperature from 0.14 Å/cycle at 150°C to 0.61 Å/cycle at 250°C [25, 26]. The ALE of HfO$_2$ also displayed very similar behavior [27]. This paper will review the recent work for Al$_2$O$_3$ ALE and examine the generality of this ALE approach for a wide range of materials.

Al$_2$O$_3$ ALE Monitored Using *in situ* QCM and FTIR Techniques

Thermal Al$_2$O$_3$ ALE has been demonstrated using *in situ* quartz crystal microbalance (QCM) and Fourier transform infrared spectroscopy (FTIR) techniques [25, 26]. The thermal Al$_2$O$_3$ ALE was observed using sequential Sn(acac)$_2$ and HF exposures. The HF source was a solution of HF-pyridine. The initial Al$_2$O$_3$ film was deposited using Al$_2$O$_3$ ALD with trimethylaluminum and H$_2$O as the reactants.

Figure 1 shows the mass changes measured by the *in situ* QCM measurements during the sequential Sn(acac)$_2$ and HF exposures at 200°C [25]. The etching of the Al$_2$O$_3$ film is linear and displays a mass change per cycle (MCPC) of -8.4 ng/(cm^2 cycle). This MCPC corresponds to an etch rate of 0.28 Å/cycle based on the Al$_2$O$_3$ ALD film density of 3.0 g/cm^3 measured using x-ray reflectivity (XRR).
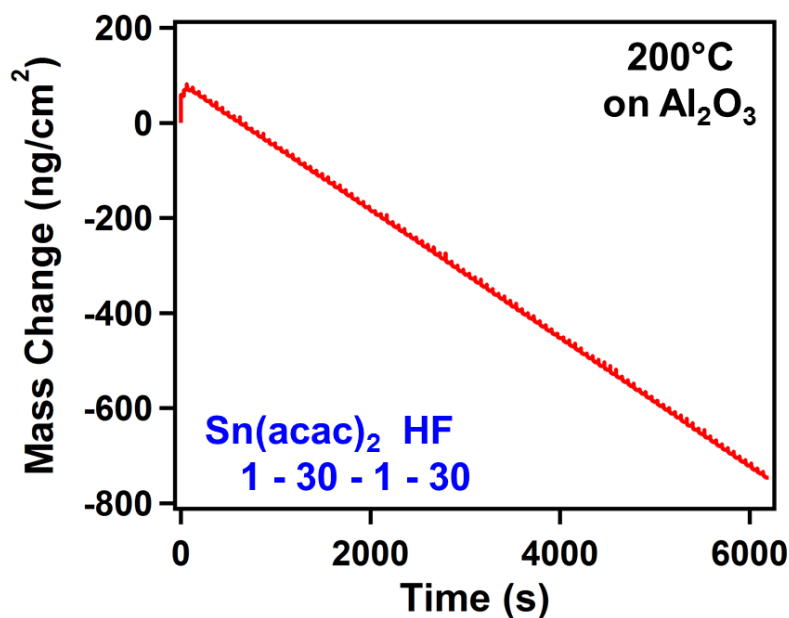

Figure 1. Mass change versus time for Al$_2$O$_3$ ALE using sequential Sn(acac)$_2$ and HF exposures at 200°C.

Additional XRR and spectroscopic ellipsometry (SE) measurements confirmed the Al$_2$O$_3$ ALE. These experiments were performed on Al$_2$O$_3$ ALD films grown on silicon wafers. Figure 2 displays the Al$_2$O$_3$ film thicknesses versus number of sequential Sn(acac)$_2$ and HF exposures at 200°C [25]. One initial Al$_2$O$_3$ ALD film was grown using 150 Al$_2$O$_3$ ALD cycles and the other initial Al$_2$O$_3$ ALD film was grown using 100 Al$_2$O$_3$ ALD cycles.
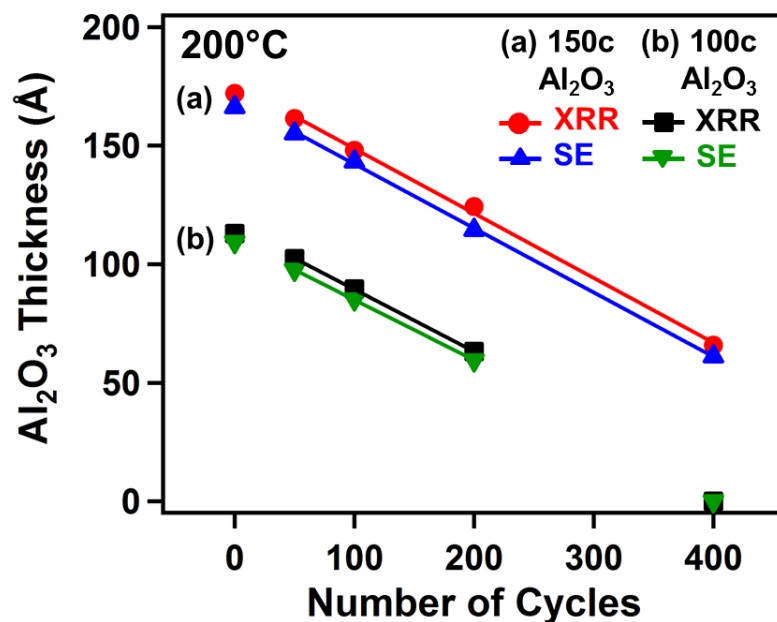
Figure 2. X-ray reflectivity and spectroscopic ellipsometry measurements of Al_2O_3 film thickness versus number of Al_2O_3 ALE cycles at 200°C for initial Al_2O_3 ALD films grown using (a) 150 Al_2O_3 ALD cycles and (b) 100 Al_2O_3 ALD cycles.
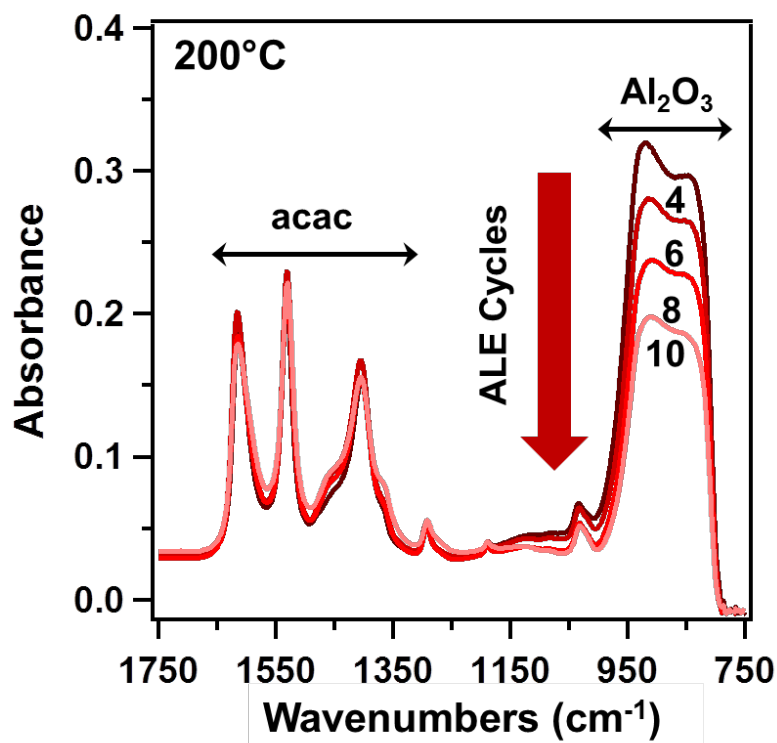

Figure 3. Infrared absorbance showing the loss of Al-O stretching vibrations in bulk Al_2O_3 versus number of Al_2O_3 ALE cycles at 200°C. These FTIR spectra were referenced to the initial ZrO_2 nanoparticles.

The XRR and SE measurements confirm that the Al_2O_3 ALE is linear. The XRR results in Figure 2 are consistent with an Al_2O_3 etch rate of 0.27 Å/cycle at 200°C [25]. The SE results in Figure 2 are also consistent with an Al_2O_3 etch rate of 0.27 Å/cycle at 200°C [25]. These measurements are in excellent agreement with the Al_2O_3 etch rate of 0.28 Å/cycle obtained from the QCM analysis at 200°C.

The Al_2O_3 ALE can also be observed using *in situ* FTIR spectroscopy analysis. In these experiments, Al_2O_3 ALD films are first grown on ZrO_2 nanoparticles [26]. Subsequently, the absorbance of the Al-O stretching vibrations is monitored versus number of sequential $Sn(acac)_2$ and HF exposures. Figure 3 shows the absorbance of the Al-O stretching vibrations versus number of sequential $Sn(acac)_2$ and HF exposures [26]. The infrared absorbance decreases progressively versus the sequential $Sn(acac)_2$ and HF exposures.
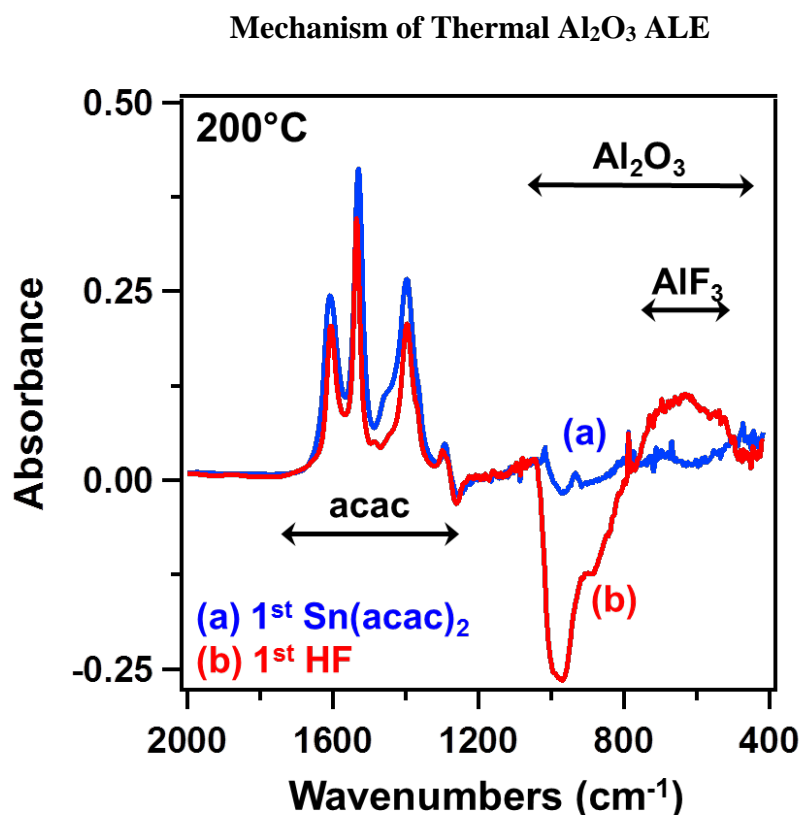
Mechanism of Thermal Al_2O_3 ALE

Figure 4. Infrared absorbance after the first $Sn(acac)_2$ exposure and first HF exposure on an Al_2O_3 film at 200°C. These FTIR spectra were referenced to the SiO_2 nanoparticles coated with the Al_2O_3 ALD film.

The FTIR spectra can also help to determine the mechanism of Al_2O_3 ALE. Figure 4 shows the infrared absorbance in the region from 400-2000 cm^{-1}. This region contains the vibrations from the acac surface species, the Al-O stretching vibrations in Al_2O_3 and the Al-F stretching vibrations in AlF_3. Figure 4a displays the infrared absorbance after the first $Sn(acac)_2$ exposure on an initial Al_2O_3 substrate [26]. This spectrum reveals acac-containing species. These acac-containing species could be $Sn(acac)_2$* from the

molecular adsorption of Sn(acac)$_2$ or Sn(acac)* and acac* from the dissociative adsorption of Sn(acac)$_2$ on Al$_2$O$_3$. The asterisks designate surface species.

Figure 4b displays the infrared absorbance after the first HF exposure following the first Sn(acac)$_2$ exposure on the initial Al$_2$O$_3$ substrate [26]. This spectrum reveals a loss of absorbance in the region corresponding to the Al-O stretching vibrations. In addition, this spectrum also shows a gain of absorbance in the region corresponding to the Al-F stretching vibrations.

The loss of absorbance from the Al-O stretching vibrations and gain of absorbance from the Al-F stretching vibrations strongly suggests that the HF exposure fluorinates the Al$_2$O$_3$ substrate. This fluorination reaction can be written as Al$_2$O$_3$ + 6HF $\rightarrow$ 2AlF$_3$ + 3H$_2$O. Thermochemical calculations indicate that this reaction is very favorable. The Gibbs free energy change for this reaction is ΔG = -58 kcal at 200°C [28].

The etching rate during Al$_2$O$_3$ ALE is also temperature dependent. Figure 5 shows QCM measurements of Al$_2$O$_3$ ALE at temperature from 150-250°C [26]. The MCPC increases with temperature from -4.1 ng/(cm^2 cycle) at 150°C to -18.3 ng/(cm^2 cycle) at 250°C. These MCPCs correspond to etch rates that vary from 0.14 Å/cycle at 150°C to 0.61 Å/cycle at 250°C. The determination of these etch rates is again based on the Al$_2$O$_3$ ALD film density of 3.0 g/cm^3.
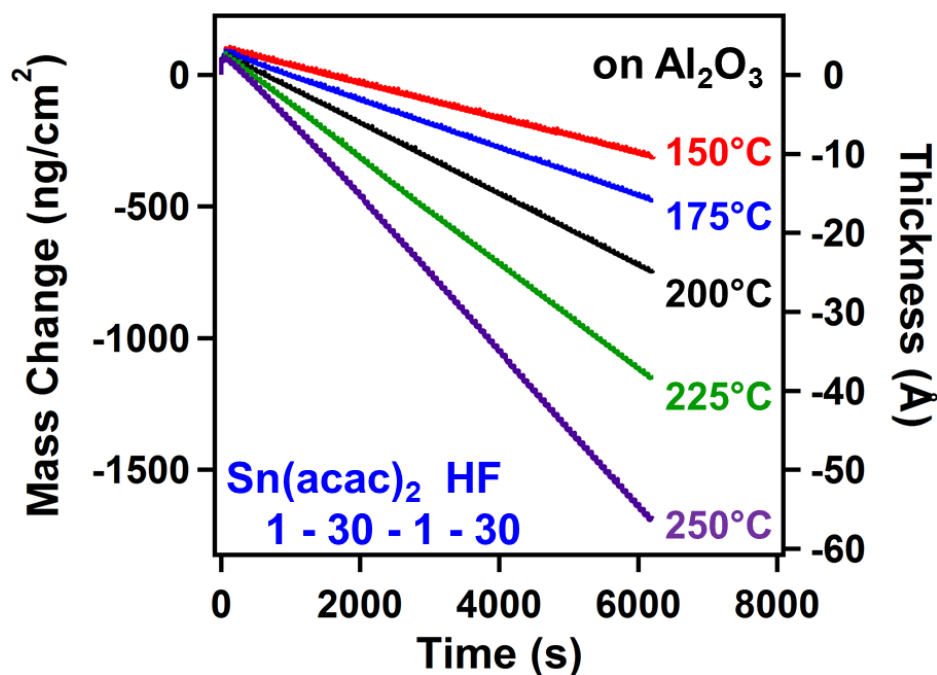
Figure 5. Mass change versus time for Al$_2$O$_3$ ALE using sequential Sn(acac)$_2$ and HF exposures at 150, 175, 200, 225 and 250°C.

The temperature dependence of Al$_2$O$_3$ ALE is also observed in the FTIR spectra after sequential Sn(acac)$_2$ and HF exposures. Figure 6 shows the FTIR difference spectra during sequential Sn(acac)$_2$ and HF exposures [26]. The growth of absorbance from the Al-F stretching vibrations after the HF exposures is larger at higher temperatures. In

addition, the removal of the absorbance from the Al-F stretching vibrations after the Sn(acac)$_2$ exposures is also larger at higher temperatures.
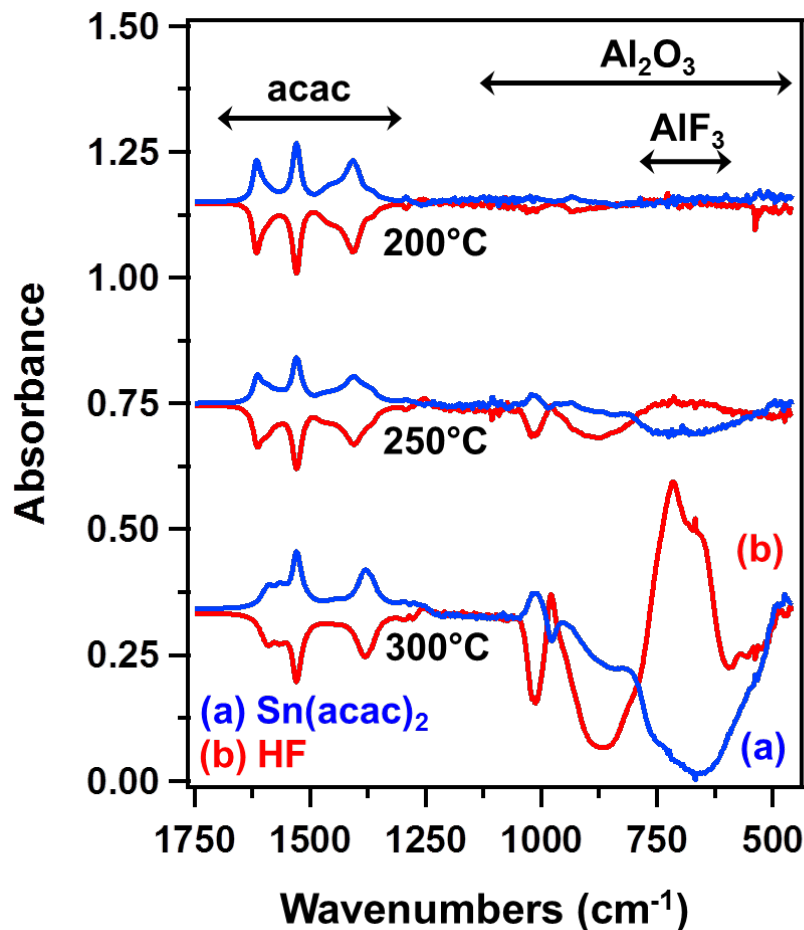

Figure 6. FTIR difference spectra during Al$_2$O$_3$ ALE at 200°C, 250°C and 300°C. The difference spectra recorded after the Sn(acac)$_2$ and HF exposures were referenced using the spectra after the previous HF and Sn(acac)$_2$ exposures, respectively.

The absorbance changes at 250°C and 300°C in Figure 6 reveal a loss of absorbance from Al-O stretching vibrations that is concurrent with the gain of absorbance from Al-F stretching vibrations. These absorbance changes again argue that the HF exposure fluorinates the Al$_2$O$_3$ substrate and forms an AlF$_3$ surface layer. The Sn(acac)$_2$ exposure is then able to remove some of this AlF$_3$ surface layer.

These FTIR results in Figure 6 and the previous FTIR results in Figure 4 suggest the following mechanism for thermal Al$_2$O$_3$ ALE. The HF exposure fluorinates the Al$_2$O$_3$ substrate to form an AlF$_3$ surface layer and volatile H$_2$O. The Sn(acac)$_2$ reactant subsequently accepts fluorine from the AlF$_3$ surface layer and donates an acac ligand to the aluminum in the AlF$_3$ surface layer to form volatile Al(acac)$_3$ or AlF(acac)$_2$ reaction products. This reaction mechanism is shown in Figure 7 assuming that Al(acac)$_3$ is the reaction product [25, 26].
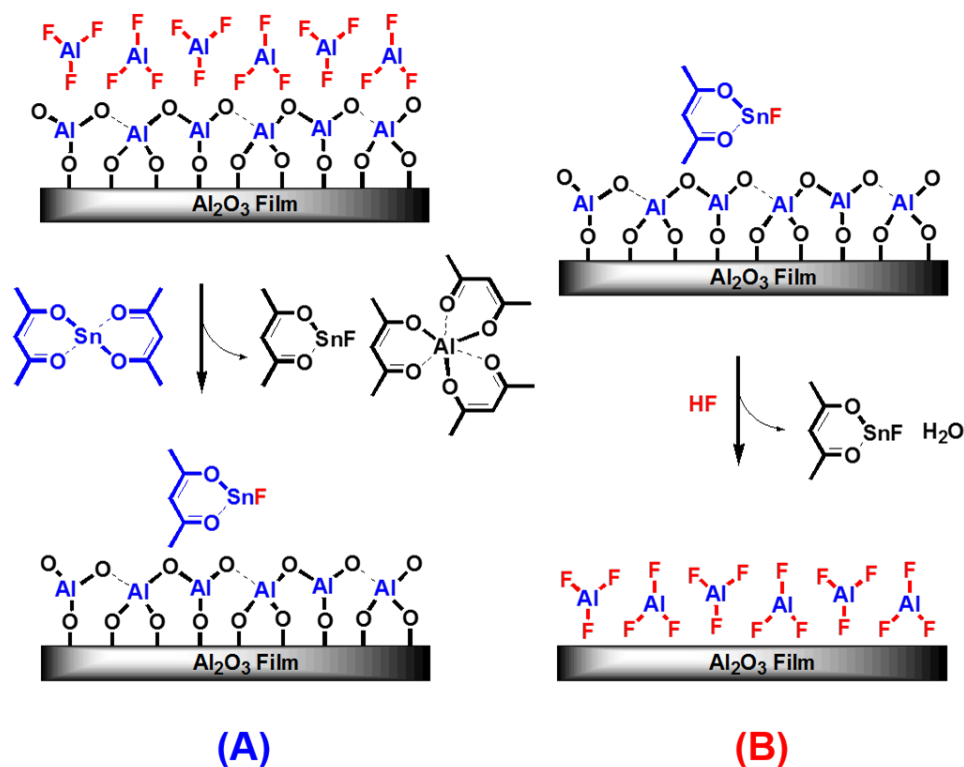
Figure 7. Schematic of the proposed surface chemistry for Al_2O_3 ALE showing (A) $Sn(acac)_2$ reaction and (B) HF reaction.

The Al_2O_3 ALE reactions can be viewed in terms of fluorination and ligand-exchange reactions. The order of the $Sn(acac)_2$ and HF exposures was also changed and the HF exposure was applied to the initial Al_2O_3 substrate before the $Sn(acac)_2$ exposure. QCM measurements revealed that this change of order did not affect the steady state Al_2O_3 ALE. There was only a small difference in the mass changes during the initial HF and $Sn(acac)_2$ exposures in the nucleation region.

The fluorination and ligand-exchange reactions can be viewed in terms of the general scheme shown in Figure 8. The HF fluorinates the Al_2O_3 substrate and forms an AlF_3 surface layer. The $Sn(acac)_2$ then accepts fluorine from the AlF_3 surface layer and donates an acac ligand to an aluminum atom in the AlF_3 surface layer. The $SnF(acac)$ and $Al(acac)_3$ reaction products lead to the etching of AlF_3.

Generality of Thermal ALE

This thermal ALE procedure is general and can be applied to many materials including metal nitrides, metal phosphides, metal arsenides and elemental metals [25]. In all cases, thermochemical calculations confirm that fluorination can lead to the formation of metal fluorides by spontaneous reactions [25]. If the metal fluorides are stable, then thin films of these materials can be etched by the subsequent ligand-exchange reaction.

Most metals have stable metal fluorides. Some exceptions are iridium, molybdenum, platinum, rhenium, tantalum and tungsten. The metal fluorides of these elements have melting points less than 100°C and will have high volatility under typical etching reaction conditions. These metals may be etched spontaneously during the fluorination reaction. Silicon and germanium are two other elements with fluorides that have melting points less than 100°C. These fluorides will also have high volatility under etching reaction conditions.
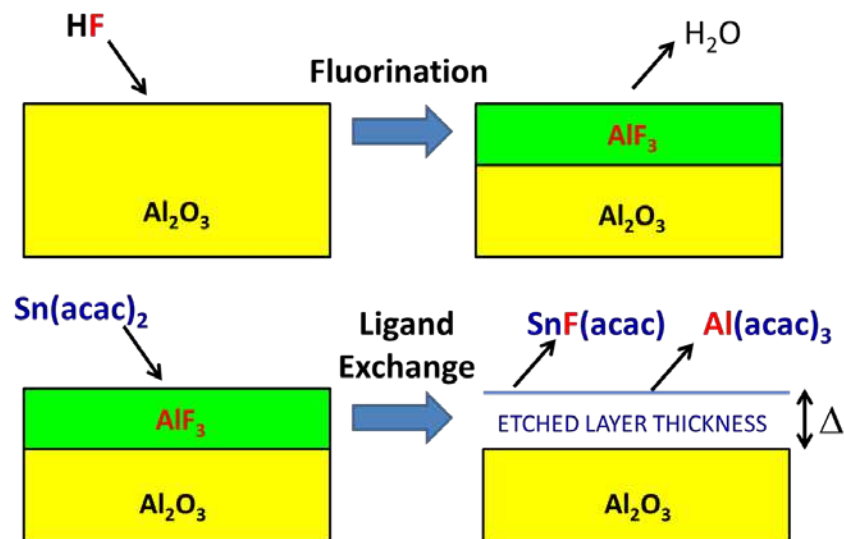

Figure 8. General schematic of the proposed surface chemistry for Al_2O_3 ALE showing (A) fluorination reaction that converts the surface of the Al_2O_3 substrate to an AlF_3 surface layer and (B) ligand-exchange reaction that leads to volatile species that removes the AlF_3 surface layer.

Conclusions

The ALE of Al_2O_3 by sequential, self-limiting thermal reactions demonstrates that new reactions are possible to etch materials with atomic layer control. These reactions are equivalent to ALD in reverse. These reactions occur spontaneously without the need for ion-enhanced or energetic neutral atom beams. The etching is linear with the number of $Sn(acac)_2$ and HF reaction cycles. Higher temperatures also lead to larger etching rates. The new capabilities provided by these sequential, self-limiting thermal reactions should be useful in nanofabrication. This new approach to thermal ALE should be particularly useful for isotropic etching.

Acknowledgments

References

1. A. Agarwal and M.J. Kushner, *J. Vac. Sci. Technol. A* **27,** 37 (2009).
2. C.T. Carver, J.J. Plombon, P.E. Romero, S. Suri, T.A. Tronic and R.B. Turkot, *ECS Journal of Solid State Science and Technology* **4,** N5005 (2015).
3. G.S. Oehrlein, D. Metzler and C. Li, *ESC Journal of Solid State Science and Technology* **4,** N5041 (2015).
4. T. Faraz, F. Roozeboom, H.C.M. Knoops and W.M.M. Kessels, *ECS Journal of Solid State Science and Technology* **4,** N5023 (2015).
5. S.M. George, *Chem. Rev.* **110,** 111 (2010).
6. M. Leskela and M. Ritala, *Angew. Chem. Int. Ed.* **42,** 5548 (2003).
7. N. Marchack and J.P. Chang, *J. Phys. D Appl. Phys.* **44,** 174011 (2011).
8. S.D. Athavale and D.J. Economou, *J. Vac. Sci. Technol. B* **14,** 3702 (1996).
9. S.D. Park, D.H. Lee and G.Y. Yeom, *Electrochem. Solid State Lett.* **8,** C106 (2005).
10. H. Sakaue, S. Iseda, K. Asami, J. Yamamoto, M. Hirose and Y. Horiike, *Jpn. J. Appl. Phys. 1* **29,** 2648 (1990).
11. J. Yamamoto, T. Kawasaki, H. Sakaue, S. Shingubara and Y. Horiike, *Thin Solid Films* **225,** 124 (1993).
12. T. Sugiyama, T. Matsuura and J. Murota, *Appl. Surf. Sci.* **112,** 187 (1997).
13. W.S. Lim, S.D. Park, B.J. Park and G.Y. Yeom, *Surf. Coat. Tech.* **202,** 5701 (2008).
14. T. Meguro, M. Hamagaki, S. Modaressi, T. Hara, Y. Aoyagi, M. Ishii and Y. Yamamoto, *Appl. Phys. Lett.* **56,** 1552 (1990).
15. T. Meguro, M. Ishii, T. Sugano, K. Gamo and Y. Aoyagi, *Appl. Surf. Sci.* **82-3,** 193 (1994).
16. S.D. Park, C.K. Oh, J.W. Bae, G.Y. Yeom, T.W. Kim, J.I. Song and J.H. Jang, *Appl. Phys. Lett.* **89,** 043109 (2006).
17. W.S. Lim, J.B. Park, J.Y. Park, B.J. Park and G.Y. Yeom, *J. Nanosci. Nanotechnol.* **9,** 7379 (2009).
18. D. Metzler, R.L. Bruce, S. Engelmann, E.A. Joseph and G.S. Oehrlein, *J. Vac. Sci. Technol. A* **32,** 020603 (2014).
19. K.S. Min, S.H. Kang, J.K. Kim, Y.I. Jhon, M.S. Jhon and G.Y. Yeom, *Microelectron. Eng.* **110,** 457 (2013).
20. J.B. Park, W.S. Lim, B.J. Park, I.H. Park, Y.W. Kim and G.Y. Yeom, *J. Phys. D Appl. Phys.* **42,** 055202 (2009).
21. J.B. Park, W.S. Lim, S.D. Park, Y.J. Park and G.Y. Yeom, *J. Korean Phys. Soc.* **54,** 976 (2009).
22. Y.Y. Kim, W.S. Lim, J.B. Park and G.Y. Yeom, *J. Electrochem. Soc.* **158,** D710 (2011).
23. W.S. Lim, Y.Y. Kim, H. Kim, S. Jang, N. Kwon, B.J. Park, J.-H. Ahn, I. Chung, B.H. Hong and G.Y. Yeom, *Carbon* **50,** 429 (2012).
24. E. Vogli, D. Metzler and G.S. Oehrlein, *Appl. Phys. Lett.* **102,** 253105 (2013).
25. Y. Lee and S.M. George, *ACS Nano* **9,** 2061 (2015).
26. Y. Lee, J.W. DuMont and S.M. George, *Chem. Mater.* **27,** 3648 (2015).
27. Y. Lee, J.W. DuMont and S.M. George, *ECS J. Solid State Sci. Technol.* **4,** N5013 (2015).
28. *HSC Chemistry*, Pori, Finland.: HSC Chemistry 5.1, Outokumpu Research Oy.